

# Quantum Criticality and Spin Liquid Phase in the Shastry-Sutherland model

Jianwei Yang,<sup>1</sup> Anders W. Sandvik,<sup>2,3,\*</sup> and Ling Wang<sup>4,†</sup>

<sup>1</sup>*Beijing Computational Science Research Center, 10 East Xibeiwang Road, Beijing 100193, China*

<sup>2</sup>*Department of Physics, Boston University, 590 Commonwealth Avenue, Boston, Massachusetts 02215, USA*

<sup>3</sup>*Beijing National Laboratory for Condensed Matter Physics and Institute of Physics, Chinese Academy of Sciences, Beijing 100190, China*

<sup>4</sup>*Department of Physics, Zhejiang University, Hangzhou 310000, China*

(Dated: April 21, 2022)

Using the density-matrix renormalization group method for the ground state and excitations of the Shastry-Sutherland spin model, we demonstrate the existence of a narrow quantum spin liquid phase between the previously known plaquette-singlet and antiferromagnetic states. Our conclusions are based on finite-size scaling of excited level crossings and order parameters. Together with previous results on candidate models for deconfined quantum criticality and spin liquid phases, our results point to a unified quantum phase diagram where the deconfined quantum-critical point separates a line of first-order transitions and a gapless spin liquid phase. The frustrated Shastry-Sutherland model is close to the critical point but slightly inside the spin liquid phase, while previously studied unfrustrated models cross the first-order line. We also argue that recent heat capacity measurements in  $\text{SrCu}_2(\text{BO}_3)_2$  show evidence of the proposed spin liquid at pressures between 2.6 and 3 GPa.

The quasi two-dimensional (2D)  $S = 1/2$  quantum magnet  $\text{SrCu}_2(\text{BO}_3)_2$  [1–3] has emerged [4–9] as the most promising realization of a deconfined quantum-critical point (DQCP) [10–12], where a state spontaneously forming a singlet pattern meets an antiferromagnetic (AF) state in a phase transition associated with fractionalized excitations (spinons). The intralayer interactions of the Cu spins correspond to the Shastry-Sutherland (SS) model [13], with highly frustrated AF interdimer ( $J$ ) and intradimer ( $J'$ ) Heisenberg couplings. The SS model has three known ground states versus  $g = J/J'$ : a dimer singlet (DS) state for small  $g$  [13], a Néel AF state for large  $g$ , and a two-fold degenerate plaquette-singlet (PS) state for  $g \in [0.68, 0.77]$  [3, 6, 14, 15].

At ambient pressure  $\text{SrCu}_2(\text{BO}_3)_2$  is in the DS phase [1, 2] but the other SS phases have been anticipated under high pressure [16]. Recent heat capacity [7, 8], neutron scattering [4], and Raman [9] experiments have indeed confirmed some variant [17, 18] of the PS phase (from 1.7 to 2.5 GPa at temperatures  $T < 2$  K) and an AF phase (between 3 and 4 GPa below 4 K). A direct PS–AF transition may then be expected between 2.6 and 3 GPa [19] at temperatures not yet reached.

Here we show that the above picture is incomplete. Using the density-matrix renormalization group (DMRG) method [20], we study the ground state and low-lying excitations of the SS model. Based on the lattice-size dependence of the level spectrum and order parameters, we conclude that a narrow gapless spin liquid (SL) phase intervenes between the PS and AF phases. In light of this finding, the absence of signs of any phase transition between 2.6 and 3 GPa [7, 8] opens the intriguing prospect of an SL phase in  $\text{SrCu}_2(\text{BO}_3)_2$ .

*DMRG calculations.*—The SS model with AF couplings  $J$  between first neighbor spins  $\langle ij \rangle$  and  $J'$  on a subset of second neighbors  $\langle ij' \rangle$  is illustrated in Fig. 1. The Hamiltonian is [13]

$$H = J \sum_{\langle ij \rangle} \mathbf{S}_i \cdot \mathbf{S}_j + J' \sum_{\langle ij' \rangle} \mathbf{S}_i \cdot \mathbf{S}_j, \quad (1)$$

here on  $L_x \times L_y$  cylinders [21, 22] with open and periodic boundaries in the  $x$  and  $y$  direction, respectively, and

$L \equiv L_y = 2n$ ,  $L_x = 2L$ . In this geometry, the model has a preferred singlet pattern which minimizes the boundary energy in the PS phase; thus the two-fold degeneracy is broken and the ground state is unique, as illustrated in Fig. 1.

We have developed efficient procedures for calculating not only the ground state with full  $SU(2)$  symmetry [23, 24], but also successively generating excited states by orthogonalizing to previous states [25–27]. Imposing stringent convergence criteria for given Schmidt number  $m$ , we have reached sufficiently large  $m$  for reliably extrapolating to discarded weight  $\epsilon_m = 0$  (Supplemental Material [28]) for  $L$  up to 10, 12, or 14 depending on quantity (energies and order parameters). Any remaining errors in the results are small on the scale of the graph symbols in the figures presented below.

We focus on the window  $g \in [0.7, 0.9]$ , which straddles the PS and AF phases. The ground state of the system is always a singlet, and we analyze the gaps  $\Delta(S)$  to the lowest excited singlet ( $S = 0$ ), triplet ( $S = 1$ ), and quintuplet ( $S = 2$ ). Finite-size crossings of excited levels with different spin are often used indicators of quantum phase transitions in spin chains [29–32], and this method was also applied to the 2D  $J$ - $Q$  [33] and  $J_1$ - $J_2$  [26, 34, 35] Heisenberg models. We here use level crossings to detect the transitions out of the PS phase and into the AF state, following Ref. 26 closely. We also study the PS

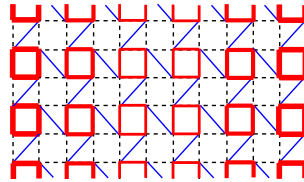


Figure 1. The SS lattice with open  $x$  and periodic  $y$  boundary conditions. The lengths  $L_x$  and  $L_y$  are both even. Nearest neighbors are coupled at strength  $J$  by Eq. (1) and the blue diagonal links represent the dimer couplings  $J'$ . The open edges break the  $\mathbb{Z}_2$  symmetry of the PS phase, thus inducing a singlet density pattern as indicated schematically by the thickness of the red lines.

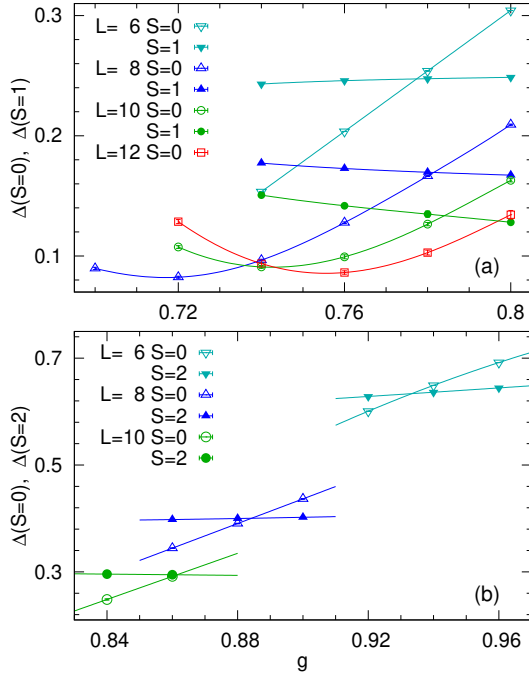


Figure 2. (a) The lowest singlet and triplet gaps vs  $g$  in the neighborhood of the expected quantum phase transition out of the PS phase. (b) The lowest singlet and quintuplet gaps for  $g$  inside the AF phase, close to its quantum phase transition. The curves are polynomial fits.

and AF order parameters to corroborate the quantum phases and phase transitions.

We graph singlet and triplet gaps in Fig. 2(a) and similarly singlet and quintuplet gaps in Fig. 2(b), in  $g$  windows where gap crossings are observed. In Fig. 3 we analyze the gap crossing points and the singlet minimum that is also observed in Fig. 2(a). Given the previous empirical observations of crossing-point drifts in 2D systems [26, 33], we graph the results versus  $1/L^2$  and find almost perfect linear behaviors. Interesting, the singlet-triplet crossing and the singlet minimum both extrapolate to  $g_{c1} \approx 0.79$ , while the singlet-quintuplet points scale to a higher value;  $g_{c2} \approx 0.82$ .

It was previously shown [26, 31] that the crossing point between the lowest singlet and quintuplet levels is a useful finite-size estimator for a quantum phase transition into an AF phase, given that the lowest  $S > 0$  states are Anderson quantum rotors, separated from the ground state by gaps  $\Delta_A(S) \propto S(S+1)/L^2$ , while the singlet excited state should be the gapped amplitude (“Higgs”) mode in the AF state [6]. In contrast, in other putative phases adjacent to the AF phase (in the SS model and many other models), the  $S = 2$  state will be above the lowest  $S = 0$  excitation. Thus, we identify the extrapolated singlet-quintuplet crossing point  $g_{c2} \approx 0.82$  with a quantum phase transition into the AF state.

Following previous work on the  $J_1$ - $J_2$  model [26], we identify the extrapolated singlet-triplet crossing point  $g_{c1} \approx 0.79$  with the transition out of the PS state. The singlet minimum by itself is consistent with the PS gap vanishing at a DQCP

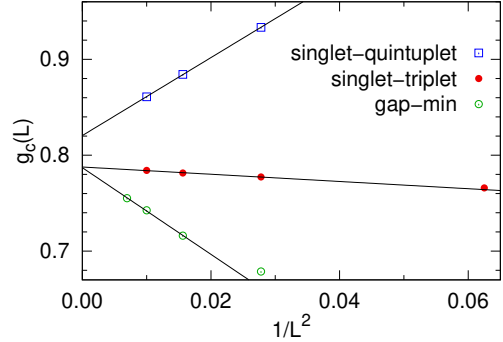


Figure 3. Locations of gap crossings and singlet minimum, with the lines showing linear-in- $1/L^2$  fits. The  $L = 4$  singlet-quintuplet point is at  $g \approx 1.1$ , falling very close to the fitted line. The extrapolated critical points are  $g_{c1} = 0.788 \pm 0.002$  and  $g_{c2} = 0.820 \pm 0.002$ .

and becoming the gapped amplitude mode in the AF phase [6]. However, an AF phase starting at  $g_{c1}$  is inconsistent with the singlet-quintuplet crossing point  $g_{c2}$ . Though the separation between the transition points  $g_{c1} \approx 0.79$  and  $g_{c2} \approx 0.82$  is small, an eventual flow toward a common point for larger systems appears unlikely, given the absence of significant corrections to the  $1/L^2$  forms in Fig. 3. Below we will show evidence for a gapless SL phase for  $g \in (g_{c1}, g_{c2})$ .

Both gap crossings match those in the  $J_1$ - $J_2$  Heisenberg model [26], where several numerical studies have reached a consensus on the existence of a gapless SL phase between dimerized and AF phases [24, 26, 34–36]. A field theory was recently proposed for this SL phase [37]. Moreover, the same level crossings were found at the transition from a critical state to either a dimerized state (singlet-triplet crossing) or an AF state (singlet-quintuplet crossing) in a frustrated Heisenberg chain with long-range interactions [26, 31]. Given these results for related models, the distinct  $g_{c1}$  and  $g_{c2}$  points suggest a gapless SL phase also in the SS model.

In Fig. 4 we analyze the size dependent gaps in and close to the putative SL phase. At  $g = 0.80$ , both the singlet and triplet gaps exhibit asymptotic  $1/L$  scaling, corresponding to a dynamic exponent  $z = 1$  inside the SL phase. At  $g = 0.76$ , in the PS phase, the singlet (and also the not shown triplet) converges exponentially to a non-zero gap, as expected in the SS model with cylindrical boundaries (Fig. 1) for which the shifted PS state is gapped by boundary energies. In the AF phase, we find convergence to a non-zero amplitude-mode energy at  $g = 0.84$ . In Fig. 4 we have fitted a polynomial in this case, which works better than an exponentially convergent form, likely due to a gapless spectrum above the lowest singlet (unlike the isolated singlet mode in the PS state).

We next study order parameters. We use the squared AF magnetization,  $m_s^2 = L^{-4} \sum_{ij} \phi_{ij} \langle \mathbf{S}_i \cdot \mathbf{S}_j \rangle$ , where  $i, j$  are sites in the central  $L \times L$  area of a  $2L \times L$  system and  $\phi_{ij} = \pm 1$  is the staggered phase. To detect PS order we define  $\mathbf{Q}_r \equiv \frac{1}{2}(\mathbf{P}_r + \mathbf{P}_r^{-1})$ , with  $\mathbf{P}_r$  a cyclic permutation operator on the four spins of a plaquette at  $r$ . Given the boundary-induced plaquette pattern (Fig. 1), we can detect the PS order

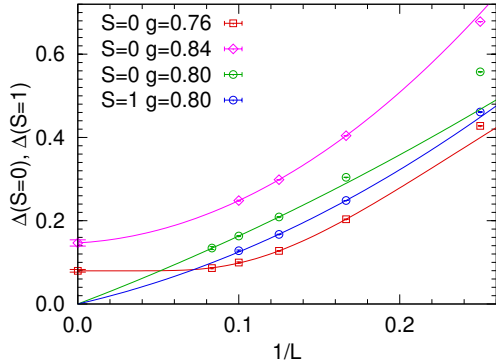


Figure 4. Gaps vs inverse system size. The singlet and triplet at  $g = 0.80$  (SL phase) have been fitted to the form  $\Delta = a/L + b/L^2$  ( $a$  and  $b$  being fitting parameters). The singlets in the PS ( $g = 0.76$ ) and AF ( $g = 0.84$ ) phases converge to non-zero values, as shown with a fit of the form  $\Delta = a + be^{-cL}$  (fitting parameters  $a, b, c$ ) in the former case and a quadratic form in the latter case.

as the difference of  $\langle \mathbf{Q}_\mathbf{r} \rangle$  on two adjacent “empty” SS plaquettes [38]. Thus, we define  $m_p = \langle \mathbf{Q}_\mathbf{R} - \mathbf{Q}_{\mathbf{R}'} \rangle$ , where  $\mathbf{R}$  and  $\mathbf{R}'$  are both close to the center of the cylinder (the landscape of  $\mathbf{Q}_\mathbf{r}$  values is shown in the Supplemental Material [28]). Both order parameters are graphed versus  $1/L$  in Fig. 5.

Second-order polynomial extrapolations of the AF order parameter in Fig. 5 show that  $m_s^2$  vanishes for  $g \approx 0.82$ , thus providing further evidence for the AF phase starting at the extrapolated singlet-quintuplet point  $g_{c2} \approx 0.82$ . The polynomial form is strictly appropriate only inside the AF phase, while at a critical point (or phase)  $m_s^2 \propto L^{-(1+\eta)}$  should instead apply asymptotically. The  $g = 0.80$  and  $0.82$  data can indeed be fitted with  $\eta \approx 0.32$  and  $\eta \approx 0.23$ , respectively. In the PS phase, polynomial fits extrapolate to unphysical negative values, which can be understood on account of the expected  $\propto L^{-2}$  asymptotic form (which, however, cannot be fitted because of large corrections).

The inset of Fig. 5 shows how PS order is stabilized only for the larger system sizes inside the PS phase, reflecting large fluctuations in small systems (as shown explicitly in Supplemental Material [28]). The central plaquettes where  $m_p$  is defined are close to the cylinder edges for small  $L$ , and only for larger  $L$  can  $m_p$  reflect a disordered bulk. Outside the PS phase the boundary-induced order close to the edges first increases with  $L$ , thus causing non-monotonic behavior as seen most clearly at  $g = 0.82$  and  $0.84$  (see also Supplementary Material [28]). At  $g = 0.80$ ,  $m_p$  for  $L = 14$  also falls below the value for  $L = 12$ , indicating that indeed  $m_p \rightarrow 0$  when  $L \rightarrow \infty$ , as it should in the SL phase.

*DQCP and unified phase diagram.*—The originally proposed DQCP is generic, reachable by tuning a single parameter [10]. Quantum Monte Carlo studies of several variants of  $J$ - $Q$  Hamiltonians [12] have indeed found direct transitions between AF and dimerized ground states [39–50]. Similar results have been obtained with related classical loop [51, 52] and dimer [53] models. In most cases, no discontinuities were observed, though unusual scaling violations point to weak

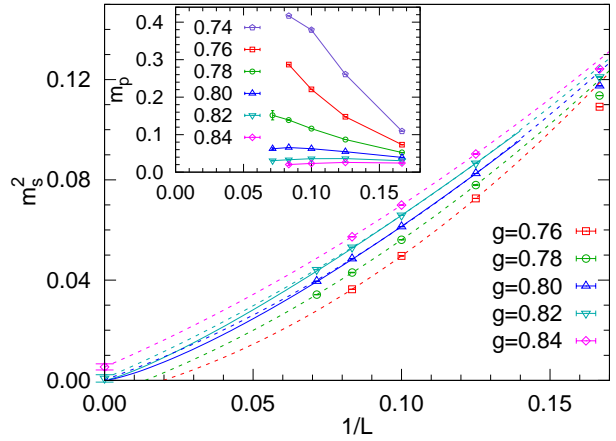


Figure 5. Squared AF order parameter vs inverse system size for several  $g$  values. The corresponding PS order parameters are shown in the inset. The dashed curves with colors matching the symbols in the main graph are second-order polynomials, while the solid curves are of the critical form  $\propto L^{-(1+\eta)}$  with  $\eta \approx 0.32$  and  $\eta \approx 0.23$  for  $g = 0.80$  and  $0.82$ , respectively. Fitting to the  $m_p$  data is not meaningful, but the non-monotonic behavior for  $g = 0.80$ – $0.84$  is explained by boundary PS order outside the PS phase (Supplemental Material [28]) and  $m_p \rightarrow 0$  for  $L \rightarrow \infty$ .

first-order transitions [40, 47, 54] or other scenarios [44, 49]. One proposal is that the DQCP is unreachable (e.g., existing only in dimensionality below 2+1) and described by a nonunitary conformal field theory (CFT) [55–61].

In some variants of the  $J$ - $Q$  model clearly first-order transitions were observed [5, 62, 63]. The Checker-Board  $J$ - $Q$  (CBJQ) model [5] (and a closely related loop model [64]) has a  $\mathbb{Z}_2$  breaking PS phase like that in the SS model. A first-order spin-flop-like transition with emergent  $O(4)$  symmetry of the combined  $O(3)$  AF and scalar PS order parameters was found, with no conventional coexistence state with tunneling barriers up to the largest length scales studied. This unusual behavior indicates close proximity to an  $O(4)$  DQCP.

Lee et al. recently considered a proxy of the excitation gap with the iDMRG method (infinite-size DMRG, where  $L_x \rightarrow \infty$  and  $L_y$  is finite), studying correlation lengths of operators with the symmetries of the excited levels of interest [6]. Following Ref. 26, they identified both crossing points discussed here (Figs. 2 and 3), but these points were not extrapolated to infinite size. It was nevertheless argued that the singlet-triplet and singlet-quintuplet crossings will drift to a common DQCP with increasing system size, in the SS model as well as in the  $J_1$ - $J_2$  model. However, in a very recent work, Shackleton et al. revisited the  $J_1$ - $J_2$  model and constructed a quantum field theory of a gapless SL phase and a DQCP separating it from the AF state [37].

The narrow SL phase found here in the SS model suggests proximity to the DQCP discussed by Lee et al [6], which most likely would be the same DQCP as the one influencing the  $O(4)$  transition in the CBJQ model [5]. Moreover, it has recently been argued that the DQCP is actually a multi-critical point [65, 66]; a second relevant scaling field with all the sym-

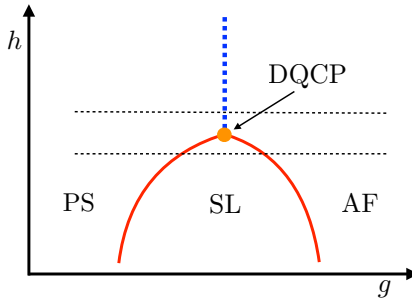


Figure 6. Unified phase diagram, where an  $O(4)$  DQCP separates a line of first-order PS–AF transitions and an extended SL phase. The PS–SL and SL–AF transition may both be continuous DQCP-like transitions. The dashed horizontal lines illustrate cuts through the phase diagram when a single parameter  $g$  is tuned; corresponding the CBJQ model (top line) and the SS model (bottom line).

metries of the Hamiltonian was detected in the conventional critical  $J$ - $Q$  model [65], and subsequently such a field was also identified in a deformed self-dual field theory [66]. In the  $J$ - $Q$  model it was found that the system flows toward a first-order transition when a certain interaction is turned on in a way maintaining a sign-free path integral [62]. It is possible that the interaction with the opposite sign could instead open up an SL phase. Taken together, all these observations suggest the unified phase diagram schematically illustrated in Fig. 6. The two parameters  $(g, h)$  correspond to two relevant symmetric fields, and in models with just one tuning parameter  $g$ , e.g., the CBJQ and SS models, either the first-order line or the SL phase is traversed. Possible ways to tune  $h$  in a model are further discussed below.

*Summary and Discussion.*—Our DMRG results can consistently be explained by a previously not anticipated SL phase between the known PS and AF phases of the SS model. The PS–SL point  $g_{c1} \approx 0.79$  is above the PS–AF point  $g_c \approx 0.765$  obtained with tensor product states [14] (where the system is infinite but the results may be affected by small tensors) but is not at significant variance with the more recent iDMRG calculation [6], where  $g_c \approx 0.77$  for  $L = 12$  and an increase in  $g_c$  with  $L$  was observed (see Table 1 of Ref. 6). The tensor technique used in Ref. 14 has a bias to ordered phases and may induce AF order in the fragile SL phase. In Ref. 6 the AF order parameter was not studied, and its appearance only at higher  $g$  may have been missed. While these works did not consider any other phase intervening between the PS and AF phases, an early field theory of the SS model within an  $1/S_i$  expansion (with  $S_i = 1/2$  being the target spin value) contains phases not detected numerically to date, including a gapped SL and a helical phase, but no gapless SL [67]. As discussed further in the Supplemental Material [28], for all values of  $g$  we find the dominant spin correlations at the Néel wave-vector  $\mathbf{k} = (\pi, \pi)$ , i.e., no helical order.

Given our SS results and the existence of a gapless SL in the square-lattice  $J_1$ - $J_2$  model [24, 26, 34–37], SLs may be ubiquitous between symmetry-breaking singlet and AF phases. The commonly studied Dirac SLs should be unstable on

square lattices and lead to DQCPs [6, 68], and the SL identified here should fall outside this framework [37]. In our scenario, in a multi-parameter model the SL can be shrunk to a multi-critical DQCP followed by a first-order direct PS–AF transition, though in principle there could be a triple point instead of the DQCP in Fig. 6, with weak first-order transitions as in the non-unitary CFT proposal [55–59, 61].

A DQCP separating a line of first-order transitions and an SL phase is a compelling scenario also considering that the  $J$ - $Q$  models can be continuously deformed into conventional frustrated models. Placing  $Q$  terms on the empty plaquettes of the SS lattice, by gradually turning off  $Q$  and turning on  $J'$  the unusual first-order PS–AF transition with emergent  $O(4)$  symmetry of the CBJQ model [5] should evolve as if the upper dashed line in Fig. 6 moved to lower  $h$ , and eventually the SS SL phase should appear. In general, we expect that many perturbations of the SS and  $J_1$ - $J_2$  models could act as the parameter  $h$  in Fig. 6, e.g., longer-range interactions or multi-spin cyclic exchange with appropriate signs.

An SL phase can explain the absence of any observed phase transition in  $\text{SrCu}_2(\text{BO}_3)_2$  at pressures 2.6–3 GPa [7, 8], between the PS and AF phases. Since  $\text{SrCu}_2(\text{BO}_3)_2$  can be synthesized with very low concentration of impurities, unlike many other potential spin liquid materials, an SL phase would be significant. A direct PS–AF transition has already been observed at high magnetic fields [8], but the nature of the transition remains unexplored. The phase diagram in Fig. 6 may also hold with  $h$  corresponding to the field strength, but with the symmetry of the AF order reduced to  $O(2)$  and potentially emergent  $O(3)$  symmetry of the DQCP [instead of  $O(4)$  at zero field] and on the adjacent direct PS–AF line.

*Acknowledgments.*—We would like to thank Frédéric Mila, Subir Sachdev, Sriram Shastry, Cenke Xu, and Yi-Zhuang You for stimulating discussions and comments, and Subir Sachdev also for sending us an early version of Ref. 37. A.W.S. was supported by the Simons Foundation under Simons Investigator Grant No. 511064. L.W. was supported by the National Key Research and Development Program of China, Grant No. 2016YFA0300603, and by the National Natural Science Foundation of China, Grants No. NSFC-11874080 and No. NSFC-11734002. The computational results presented here were achieved partially using Tianhe-2JK computing time awarded by the Beijing Computational Science Research Center (CSRC).

\* sandvik@bu.edu

† lingwangqs@zju.edu.cn

- [1] H. Kageyama, K. Yoshimura, R. Stern, N. V. Mushnikov, K. Onizuka, M. Kato, K. Kosuge, C. P. Slichter, T. Goto, and Y. Ueda, Exact Dimer Ground State and Quantized Magnetization Plateaus in the Two-Dimensional Spin System  $\text{SrCu}_2(\text{BO}_3)_2$ , *Phys. Rev. Lett.* **82**, 3168 (1999).
- [2] S. Miyahara and K. Ueda, Exact Dimer Ground State of the Two Dimensional Heisenberg Spin System  $\text{SrCu}_2(\text{BO}_3)_2$ ,

Phys. Rev. Lett. **82**, 3701 (1999).

[3] A. Koga and N. Kawakami, Quantum Phase Transitions in the Shastry-Sutherland Model for  $\text{SrCu}_2(\text{BO}_3)_2$ , Phys. Rev. Lett. **84**, 4461 (2000).

[4] M. Zayed, Ch. Rüegg, J. Larrea, A. M. Läuchli, C. Panagopoulos, S. S. Saxena, M. Ellerby, D. McMorr, Th. Strässle, S. S. Klotz, G. Hamel, R. A. Sadykov, V. Pomjakushin, M. Boehm, M. Jiménez-Ruiz, A. Schneidewin, E. Pomjakushin, M. Stincaciu, K. Conder, and H. M. Rønnow, 4-spin plaquette singlet state in the Shastry-Sutherland compound  $\text{SrCu}_2(\text{BO}_3)_2$ , Nature Phys. **13**, 962 (2017).

[5] B. Zhao, P. Weinberg, and A. W. Sandvik, Symmetry enhanced first-order phase transition in a two-dimensional quantum magnet, Nature Phys. **15**, 678 (2019).

[6] J. Y. Lee, Y.-Z. You, S. Sachdev, and A. Vishwanath, Signatures of a Deconfined Phase Transition on the Shastry-Sutherland Lattice: Applications to Quantum Critical  $\text{SrCu}_2(\text{BO}_3)_2$ , Phys. Rev. X **9**, 041037 (2019).

[7] J. Guo, G. Sun, B. Zhao, L. Wang, W. Hong, V. A. Sidorov, N. Ma, Q. Wu, S. Li, Z. Y. Meng, A. W. Sandvik, and L. Sun, Quantum Phases of  $\text{SrCu}_2(\text{BO}_3)_2$  from High-Pressure Thermodynamics, Phys. Rev. Lett. **124**, 206602 (2020).

[8] J. Larrea Jiménez, S. P. G. Crone, E. Fogh, M. E. Zayed, R. Lortz, E. Pomjakushina, K. Conder, A. M. Läuchli, L. Weber, S. Wessel, A. Honecker, B. Normand, Ch. Rüegg, P. Corboz, H. M. Rønnow, and F. Mila, A quantum magnetic analogue to the critical point of water, Nature **592**, 370 (2021).

[9] S. Bettler, L. Stoppel, Z. Yan, S. Gvasaliya, and A. Zheludev, Sign switching of dimer correlations in  $\text{SrCu}_2(\text{BO}_3)_2$  under hydrostatic pressure, Phys. Rev. Research **2**, 012010(R) (2020).

[10] T. Senthil, A. Vishwanath, L. Balents, S. Sachdev, and M. P. A. Fisher, Deconfined Quantum Critical Points, Science **303**, 1490 (2004).

[11] S. Sachdev, Quantum magnetism and criticality, Nature Phys. **4**, 173 (2008).

[12] A. W. Sandvik, Evidence for Deconfined Quantum Criticality in a Two-Dimensional Heisenberg Model with Four-Spin Interactions, Phys. Rev. Lett. **98**, 227202 (2007).

[13] B. S. Shastry and B. Sutherland, Exact ground state of a quantum mechanical antiferromagnet, Physica B+C **108**, 1069 (1981).

[14] P. Corboz and F. Mila, Tensor network study of the Shastry-Sutherland model in zero magnetic field, Phys. Rev. B **87**, 115144 (2013).

[15] H. Nakano and T. Sakai, Third Boundary of the Shastry-Sutherland Model by Numerical Diagonalization, J. Phys. Soc. Jpn. **87**, 123702 (2018).

[16] T. Waki, K. Arai, M. Takigawa, Y. Saiga, Y. Uwatoko, H. Kageyama, and Y. Ueda, A novel ordered phase in  $\text{SrCu}_2(\text{BO}_3)_2$  under high pressure, J. Phys. Soc. Jpn. **76**, 073710 (2007).

[17] C. Boos, S. P. G. Crone, I. A. Niesen, P. Corboz, K. P. Schmidt, and F. Mila, Competition between intermediate plaquette phases in  $\text{SrCu}_2(\text{BO}_3)_2$  under pressure, Phys. Rev. B **100**, 140413 (2019).

[18] Z. Shi, S. Dissanayake, P. Corboz, W. Steinhardt, D. Graf, D. M. Silevitch, H. A. Dabkowska, T. F. Rosenbaum, F. Mila, and S. Haravifard, Phase diagram of the Shastry-Sutherland Compound  $\text{SrCu}_2(\text{BO}_3)_2$  under extreme combined conditions of field and pressure, arXiv:2107.02929.

[19] G. Sun, N. Ma, B. Zhao, A. W. Sandvik, and Z. Y. Meng, Emergent  $O(4)$  symmetry at the phase transition from plaquette-singlet to antiferromagnetic order in quasi-two-dimensional quantum magnets, Chin. Phys. B **30**, 067505 (2021).

[20] S. R. White, Density Matrix Formulation for Quantum Renormalization Groups, Phys. Rev. Lett. **69**, 2863 (1992).

[21] U. Schollwöck, The density-matrix renormalization group in the age of matrix product states, Ann. Phys. (Amsterdam) **326**, 96 (2011).

[22] E. M. Stoudenmire and S. R. White, Real-space parallel density matrix renormalization group, Phys. Rev. B **87**, 155137 (2013).

[23] A. Weichselbaum, Non-abelian symmetries in tensor networks: A quantum symmetry space approach, Ann. Phys. (Amsterdam) **327**, 2972 (2012).

[24] S.-S. Gong, W. Zhu, D. N. Sheng, O. I. Motrunich, and M. P. A. Fisher, Plaquette Ordered Phase and Quantum Phase Diagram in the Spin-1/2  $J_1$ - $J_2$  Square Heisenberg Model, Phys. Rev. Lett. **113**, 027201 (2014).

[25] I. P. McCulloch, From density-matrix renormalization group to matrix product states, J. Stat. Mech. **2007**, P10014 (2007).

[26] L. Wang and A. W. Sandvik, Critical Level Crossings and Gapless Spin Liquid in the Square-Lattice Spin-1/2  $J_1$ - $J_2$  Heisenberg Antiferromagnet, Phys. Rev. Lett. **121**, 107202 (2018).

[27] M. Lemm, A. W. Sandvik, and L. Wang, Existence of a Spectral Gap in the Affleck-Kennedy-Lieb-Tasaki Model on the Hexagonal Lattice, Phys. Rev. Lett. **124**, 177204 (2020).

[28] See Supplemental material for DMRG convergence procedures and extrapolations, the 2D real-space landscape of PS ordering, and the spin structure factor.

[29] K. Nomura and K. Okamoto, Fluid-dimer critical point in  $S = 1/2$  antiferromagnetic Heisenberg chain with next nearest neighbor interactions, Phys. Lett. A **169**, 433 (1992).

[30] S. Eggert, Numerical evidence for multiplicative logarithmic corrections from marginal operators, Phys. Rev. B **54**, R9612 (1996).

[31] A. W. Sandvik, Ground States of a Frustrated Quantum Spin Chain with Long-Range Interactions, Phys. Rev. Lett. **104**, 137204 (2010).

[32] H. Suwa and S. Todo, Generalized Moment Method for Gap Estimation and Quantum Monte Carlo Level Spectroscopy, Phys. Rev. Lett. **115**, 080601 (2015).

[33] H. Suwa, A. Sen, and A. W. Sandvik, Level spectroscopy in a two-dimensional quantum magnet: Linearly dispersing spinons at the deconfined quantum critical point, Phys. Rev. B **94**, 144416 (2016).

[34] Y. Nomura and M. Imada, Dirac-type nodal spin liquid revealed by machine learning, Phys. Rev. X **11**, 031034 (2021).

[35] F. Ferrari and F. Becca, Gapless spin liquid and valence-bond solid in the  $J_1$ - $J_2$  Heisenberg model on the square lattice: Insights from singlet and triplet excitations, Phys. Rev. B **102**, 014417 (2020).

[36] S. Morita, R. Kaneko, and M. Imada, Quantum spin liquid in spin 1/2  $J_1$ - $J_2$  Heisenberg model on square lattice: Many-variable variational Monte Carlo study combined with quantum-number projections, J. Phys. Soc. Jpn. **84**, 024720 (2015).

[37] H. Shackleton, A. Thomson, and S. Sachdev, Deconfined criticality and a gapless  $\mathbb{Z}_2$  spin liquid in the square lattice antiferromagnet, Phys. Rev. B **104**, 045110 (2021).

[38] B. Zhao, J. Takahashi, and A. W. Sandvik, Comment on “Gapless spin liquid ground state of the spin-1  $J_1$ - $J_2$  Heisenberg model on square lattices”, Phys. Rev. B **101**, 157101 (2020).

[39] R. G. Melko and R. K. Kaul, Scaling in the Fan of an Unconventional Quantum Critical Point, Phys. Rev. Lett. **100**, 017203 (2008).

[40] F.-J. Jiang, M. Nfyeler, S. Chandrasekharan, and U.-J. Wiese, From an antiferromagnet to a valence bond solid: evidence for a first-order phase transition, J. Stat. Mech.: Theory Exp. **2008**,

P02009 (2008).

[41] J. Lou, A. W. Sandvik, and N. Kawashima, Antiferromagnetic to valence-bond-solid transitions in two-dimensional SU(N) Heisenberg models with multispin interactions, *Phys. Rev. B* **80**, 180414 (R) (2009).

[42] A. W. Sandvik, Continuous Quantum Phase Transition between an Antiferromagnet and a Valence-Bond Solid in Two Dimensions: Evidence for Logarithmic Corrections to Scaling, *Phys. Rev. Lett.* **104**, 177201 (2010).

[43] R. K. Kaul, Quantum criticality in SU(3) and SU(4) antiferromagnets, *Phys. Rev. B* **84**, 054407 (2011).

[44] A. W. Sandvik, Finite-size scaling and boundary effects in two-dimensional valence-bond solids, *Phys. Rev. B* **85**, 134407 (2012).

[45] M. S. Block, R. G. Melko, and R. K. Kaul, Fate of  $\mathbb{CP}^{N-1}$  Fixed Points with  $q$  Monopoles, *Phys. Rev. Lett.* **111**, 137202 (2013).

[46] K. Harada, T. Suzuki, T. Okubo, H. Matsuo, J. Lou, H. Watanabe, S. Todo, and N. Kawashima, Possibility of deconfined criticality in SU(N) Heisenberg models at small N, *Phys. Rev. B* **88**, 220408(R) (2013).

[47] K. Chen, Y. Huang, Y. Deng, A. B. Kuklov, N. V. Prokof'ev, and B. V. Svistunov, Deconfined Criticality Flow in the Heisenberg Model with Ring-Exchange Interactions, *Phys. Rev. Lett.* **110**, 185701 (2013).

[48] S. Pujari, F. Alet, and K. Damle, Transitions to valence-bond solid order in a honeycomb lattice antiferromagnet, *Phys. Rev. B* **91**, 104411 (2015).

[49] H. Shao, W. Guo, A. W. Sandvik, Quantum criticality with two length scales, *Science* **352**, 213 (2016).

[50] A. W. Sandvik and B. Zhao, Consistent scaling exponents at the deconfined quantum-critical point, *Chin. Phys. Lett.* **37**, 057502 (2020).

[51] A. Nahum, P. Serna, J. T. Chalker, M. Ortúñ, and A. M. Somoza, Emergent SO(5) Symmetry at the Néel to Valence-Bond-Solid Transition, *Phys. Rev. Lett.* **115**, 267203 (2015).

[52] A. Nahum, J. T. Chalker, P. Serna, M. Ortúñ, and A. M. Somoza, Deconfined Quantum Criticality, Scaling Violations, and Classical Loop Models, *Phys. Rev. X* **5**, 041048 (2015).

[53] G. Sreejith, S. Powell, and A. Nahum, Emergent SO(5) symmetry at the columnar ordering transition in the classical cubic dimer model, *Phys. Rev. Lett.* **122**, 080601 (2019).

[54] Z. Wang, M. P. Zaletel, R. S. K. Mong, and F. F. Assaad, Phases of the (2+1) dimensional SO(5) non-linear sigma model with topological term, *Phys. Rev. Lett.* **126**, 045701 (2021).

[55] C. Wang, A. Nahum, M. A. Metlitski, C. Xu, and T. Senthil, Deconfined Quantum Critical Points: Symmetries and Dualities, *Phys. Rev. X* **7**, 031051 (2017).

[56] V. Gorbenko, S. Rychkov, and B. Zan, Walking, weak first-order transitions, and complex CFTs, *J. High Energy Phys.* **2018**, 108 (2018).

[57] V. Gorbenko, S. Rychkov, and B. Zan, Walking, Weak first-order transitions, and Complex CFTs II. Two-dimensional Potts model at  $Q > 4$ , *SciPost Phys.* **5**, 050 (2018).

[58] R. Ma and C. Wang, A theory of deconfined pseudo-criticality, *Phys. Rev. B* **102**, 020407 (2020).

[59] A. Nahum, Note on Wess-Zumino-Witten models and quasi-universality in 2+1 dimensions, *Phys. Rev. B* **102**, 201116(R) (2020).

[60] Z. Li, Solving  $\text{QED}_3$  with Conformal Bootstrap, *arXiv:1812.09281*.

[61] Y.-C. He, J. Rong, and N. Su, Non-Wilson-Fisher kinks of  $O(N)$  numerical bootstrap: from the deconfined phase transition to a putative new family of CFTs, *SciPost Phys.* **10**, 115 (2021).

[62] B. Zhao, J. Takahashi, and A. W. Sandvik, Tunable deconfined quantum criticality and interplay of different valence-bond solid phases, *Chin. Phys. B* **29**, 057506 (2020).

[63] J. Takahashi and A. W. Sandvik, Valence-bond solids, vestigial order, and emergent SO(5) symmetry in a two-dimensional quantum magnet, *Phys. Rev. Research* **2**, 033459 (2020).

[64] P. Serna and A. Nahum, Emergence and spontaneous breaking of approximate  $O(4)$  symmetry at a weakly first-order deconfined phase transition, *Phys. Rev. B* **99**, 195110 (2019).

[65] B. Zhao, J. Takahashi, and A. W. Sandvik, Multicritical Deconfined Quantum Criticality and Lifshitz Point of a Helical Valence-Bond Phase, *Phys. Rev. Lett.* **125**, 257204 (2020).

[66] D.-C. Lu, C. Xu, and Y.-Z. You, Self-Duality Protected Multi-Criticality in Deconfined Quantum Phase Transitions, *arXiv:2104.05147*.

[67] C. H. Chung, J. B. Marston, and S. Sachdev, Quantum phases of the Shastry-Sutherland antiferromagnet: Application to  $\text{SrCu}_2(\text{BO}_3)_2$ , *Phys. Rev. B* **64**, 134407 (2001).

[68] X.-Y. Song, Y.-C. He, A. Vishwanath, and C. Wang, From Spinon Band Topology to the Symmetry Quantum Numbers of Monopoles in Dirac Spin Liquids, *Phys. Rev. X* **10**, 011033 (2020).

## Supplemental Material

### Quantum Criticality and Spin Liquid Phase in the Shastry-Sutherland model

Jianwei Yang,<sup>1</sup>, Anders W. Sandvik,<sup>2,3,\*</sup>, Ling Wang<sup>4,†</sup>

<sup>1</sup> *Beijing Computational Science Research Center, 10 East Xibeiwang Road, Beijing 100193, China*

<sup>2</sup> *Department of Physics, Boston University, 590 Commonwealth Avenue, Boston, Massachusetts 02215, USA*

<sup>3</sup> *Beijing National Laboratory for Condensed Matter Physics*

*and Institute of Physics, Chinese Academy of Sciences, Beijing 100190, China*

<sup>4</sup> *Department of Physics, Zhejiang University, Hangzhou 310000, China*

\* e-mail: sandvik@bu.edu, † lingwangqs@zju.edu.cn

Here we present additional results in support of the conclusions drawn in the main paper. In Sec. 1 we discuss the DMRG procedures and illustrate the convergence properties and extrapolations of energies and order parameters. In Sec. 2 we present 2D plots of the PS order “landscape” and discuss the effects of the open  $x$  boundaries of the cylindrical lattices, including an explanation for the nonmonotonic behavior of the PS order parameter for  $g \geq 0.80$  in Fig. 5. In Sec. 3 we present the static spin structure factor in the full wave-vector space, which shows no evidence of helical magnetic correlations in the SS model.

#### 1. DMRG convergence and extrapolations

In order to systematically approach the correct ground states and excitations in the DMRG calculations, we carry out calculations for several numbers  $m$  of Schmidt states, until either  $m$  is sufficiently large for the discarded weight  $\epsilon$  to be negligible (in case of the smaller system sizes considered here) or sufficiently small for reliably extrapolating to  $\epsilon = 0$  (for the largest system sizes). The discarded weight is defined in the standard way as the sum of discarded eigenvalues of the reduced density matrix [21, 22].

After an initial calculation for small  $m$ , each subsequent calculation is started from either a previously well converged calculation for a smaller  $m$  and the same  $g$  value, or one for a nearby  $g$  value and the same  $m$ . For a given  $m$ , we demand that the energy difference (not divided by the system volume) between two successive updating sweeps is less than  $10^{-6}$ . We then check the convergence of the energies and other quantities as a function of the discarded weight  $\epsilon$  (which depends on  $m$ , with  $\epsilon \rightarrow 0$  as  $m \rightarrow \infty$ ).

Our DMRG program is implemented with full SU(2) symmetry [23, 24], and we can therefore target the ground state of any sector of total spin  $S$ . Given that the lowest ground state among these has  $S = 0$  and we are also interested in the lowest  $S = 0$  excitation, in this sector we apply the technique of orthogonalizing to the previously calculated ground state in order to target the lowest excited  $S = 0$  state [25–27].

##### A. Cylindrical $2L \times L$ lattices

In Fig. S1 we show the lowest two  $S = 0$  energies as well as the lowest  $S = 1$  energy for system sizes  $L = 6, 8, 10$ , and 12, in the important case of  $g = 0.80$  (inside the new gapless SL phase). For the challenging  $L = 12$  system, we used  $m$  up

to 9000 for the  $S = 0$  ground state and up to  $m = 10000$  for the excited singlet. We do not have sufficiently good triplet results for  $L = 12$  and therefore only show  $S = 1$  results for the smaller systems in Fig. S1.

For  $L = 6$ , the calculation for the largest  $m$  already has an extremely small discarded weight, and it is not necessary to further extrapolate the results. We nevertheless show extrapolations for all system sizes in Fig. S1. While the exact form of the error as a function of  $\epsilon$  in the DMRG method is not known, in all cases for which data are presented in the main paper our results are sufficiently converged for the extrapolated values to not be very sensitive to the fitting form used. We have found that the energies for small  $\epsilon$  are well described by third-order polynomials without linear term. Thus, in Fig. S1 all data are fitted to such a form.

In the case of the order parameters, we find that polynomial fits work well in general (here including the linear terms). We typically use quadratic or third-order forms. Examples at  $g = 0.8$  for the two largest system sizes,  $L = 12$  and  $L = 14$ , are shown in Fig. S2. Here we observe nonmonotonic behavior of the AF order parameter  $m_s^2$  for  $L = 14$  in Fig. S2(c). For the small  $\epsilon$  values (large  $m$ ) used in the extrapolations, we have found such nonmonotonic behavior of the largest systems for  $g$  only outside the AF phase.

We point out that the  $m_s^2$  data points for  $L = 14$  in Fig. S2(c) only exhibit nonmonotonicity in the two points for smallest  $\epsilon$ , but even when these points are excluded the fit still results in a nonmonotonic polynomial. Hence, we judge this behavior as stable and the extrapolation as reliable. It should also be noted that the overall range of the  $y$ -axis of Fig. S2(c) represents a very small relative change in the value, and the uncertainties in the extrapolation for this case (less than 0.3% between different extrapolations) do not impact the conclusions drawn on the basis of the data in Fig. 5.

As seen in Fig. S2, the PS order parameter shows much

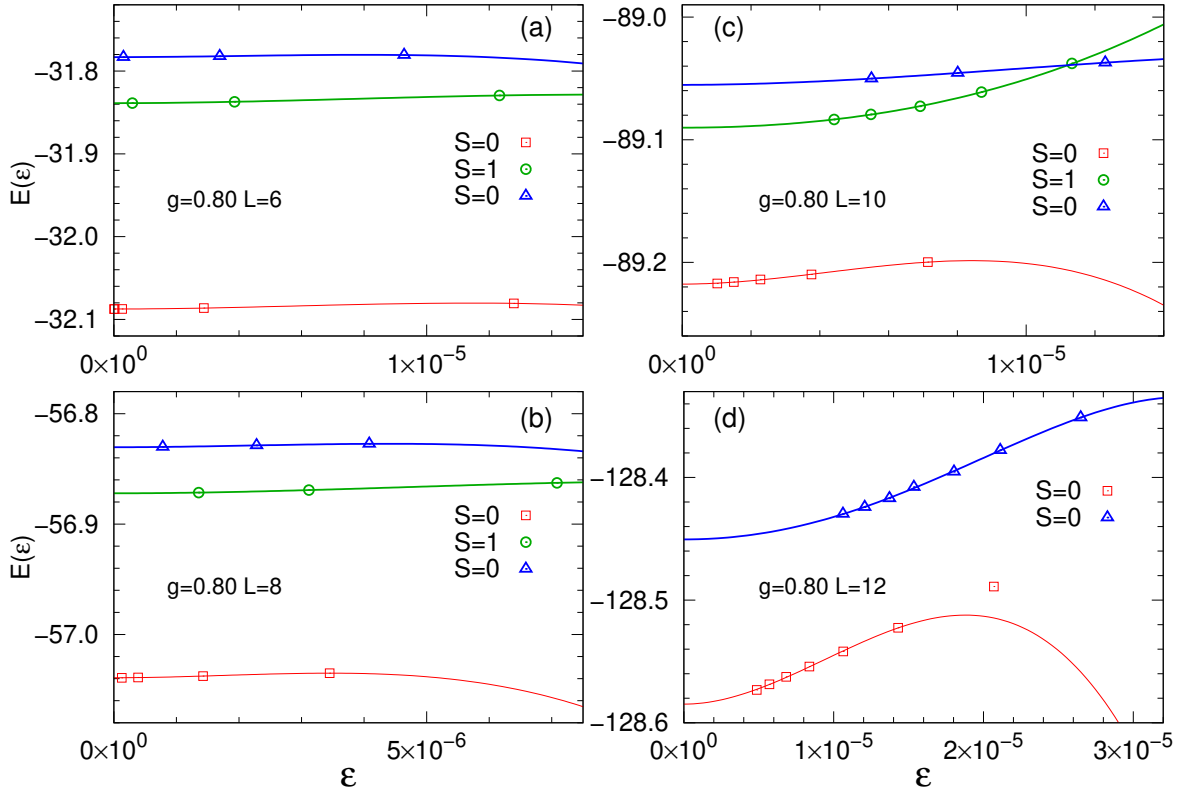


Figure S1. Examples of extrapolations of DMRG energies to vanishing discarded weight  $\epsilon$  for the SS model with  $g = 0.8$ . For each of the system sizes  $L = 6, 8, 10, 12$  in panels (a)-(d), the two lowest singlets are shown (squares and triangles) along with the lowest triplet (circles), except for  $L = 12$ , for which we do not have sufficiently well converged triplet data. The fitted curves are of the form  $E(\epsilon) = E(0) + a\epsilon^2 + b\epsilon^3$ , with  $E(0)$ ,  $a$ , and  $b$  optimized parameters.

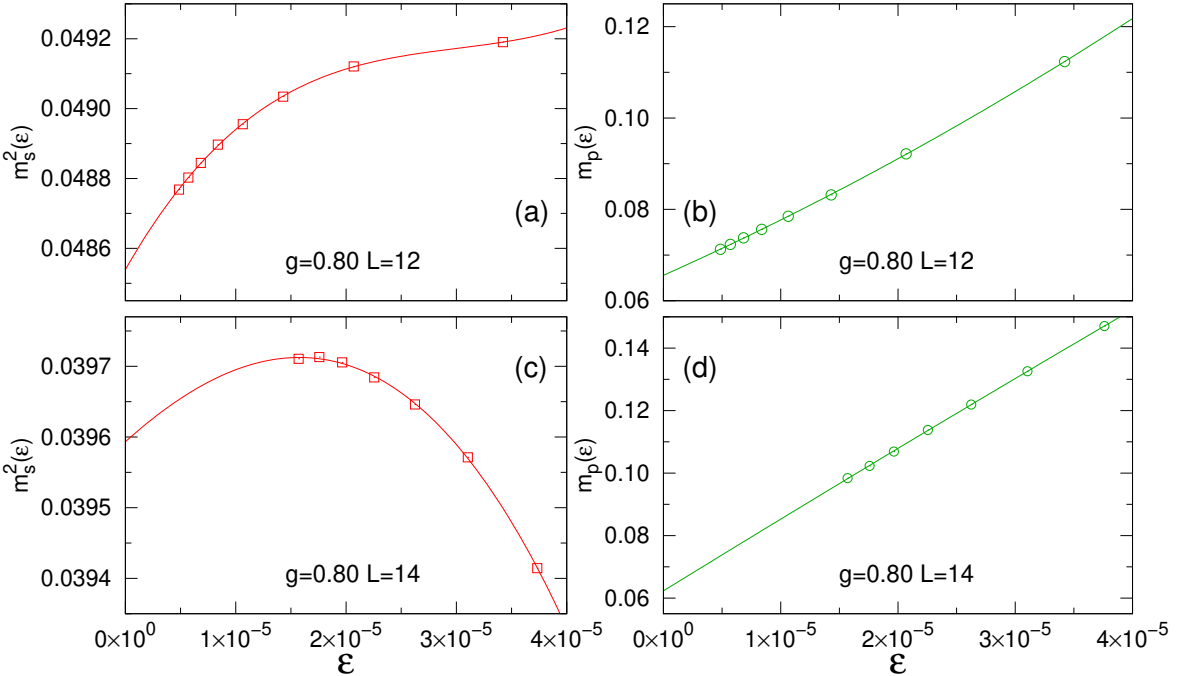


Figure S2. Examples of extrapolations of DMRG results for the AF and PS order parameters in the ground state of the SS model at  $g = 0.8$ . Results for system size  $L = 12$  are shown in (a) and (b), and corresponding results for  $L = 14$  are shown in (c) and (d). The fitted curves are quadratic polynomials in (a), (c) and cubic polynomials in (b), (d).

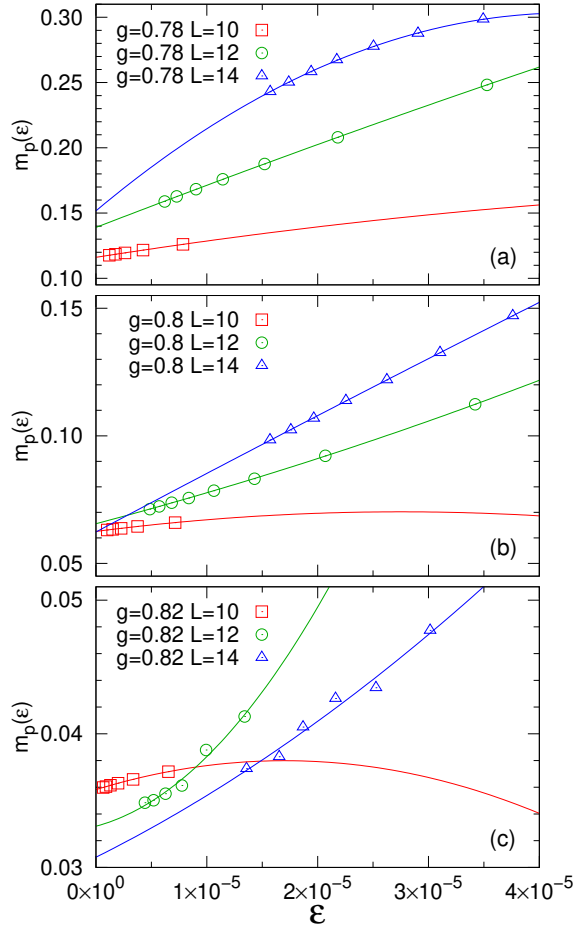


Figure S3. Plaquette order parameter vs discarded weight for (a)  $g = 0.78$ , (b)  $g = 0.80$ , and (c)  $g = 0.82$ . Each panel shows results for system sizes  $L = 10, 12, 14$ , and the curves are second-order polynomial fits used for extrapolating to  $\epsilon = 0$ . The scatter of the  $L = 14$  data (and to a lesser extent for  $L = 12$ ) in (c) originates from incomplete convergence at the Lanczos stage of the DMRG calculation for some of the points. These errors are reflected in the final error bars of the extrapolated  $m_p$  value.

larger overall dependence on  $\epsilon$  than does the AF order parameter. An important aspect of the PS order, discussed in the context of the inset of Fig. 5 in the main paper, is that its size dependence is nonmonotonic outside the PS phase; in the SL phase as well as in the AF phase close to the SL transition. In Sec. 2 we will further illustrate how this behavior originates from the cylindrical boundary conditions. To further illustrate the nonmonotonic behavior and its robustness in the  $\epsilon$  extrapolations, in Fig. S3 we show  $m_p$  results for the three largest system sizes,  $L = 10, 12, 14$ , for three values of  $g$  in and close to the SL phase. The nonmonotonic size dependence of the  $\epsilon \rightarrow 0$  values is clear for  $g = 0.82$ , and also for  $g = 0.80$  does this trend begin to appear. In the case of  $g = 0.78$ , the extrapolated order parameter only grows with  $L$ .

Based on only these data, it is of course not possible to exclude a maximum of the  $\epsilon \rightarrow 0$  values versus  $L$  followed by an eventual decrease to 0 for larger system sizes also for

$g = 0.78$ . However, the other results in the main paper show that this  $g$  value is inside the PS phase, and, therefore,  $m_p$  should flatten out to take a finite value if  $L$  is further increased (as is seen for still smaller  $g$  values in Fig. 5 in the main paper). The observed nonmonotonic behavior outside the PS phase (with its physical explanation in Sec. 2 below) allows us to put an upper bound on the extent of the PS phase,  $g_{c1} < 0.80$ , which is consistent with the SL phase boundaries in Fig. 3 of the main paper.

### B. $6 \times 6$ periodic system

To further illustrate the soundness of the extrapolation procedures and our methods of estimating the errors of the  $\epsilon \rightarrow 0$  energies and order parameters, we next consider a  $6 \times 6$  lattice with fully periodic (toroidal) boundary condition. Its eigenenergies for the ground state, the first singlet and triplet excitations, as well as the ground state order parameters, were obtained by Lanczos exact diagonalization. Using DMRG with SU(2) symmetry, we computed the corresponding set of variational energies and order parameters as a function of discarded weight  $\epsilon$  using several bond dimensions  $m$ . Even though the Hilbert space here is small enough for Lanczos diagonalization, the convergence properties for moderate values of  $m$  are very similar to those discussed above for the larger cylindrical lattices. Extrapolations as performed above can therefore serve as a bench-mark for the reliability of the procedures.

Figure S4(a) shows variational energies for the  $6 \times 6$  SS lattice at  $g = 0.80$  obtained by SU(2) DMRG with bond dimensions  $m = 800, 1200, 2000, \text{adn } 3000$ . The fitting function is a third-order polynomial, again without the linear term ( $E = a + b\epsilon^2 + c\epsilon^3$ ). For a reasonable definition of the error of extrapolation to  $\epsilon \rightarrow 0$ , we take the difference between extrapolated energies based on the largest three  $m$  values, shown with colored curves in Fig. S4(a), and all four points, shown with black curves. The colored dashed horizontal lines mark the exact energies, which are  $E_0 = -16.263112$ ,  $E_T = -15.985471$ ,  $E_S = -15.910097$ , for the ground state, singlet excitation, and triplet excitation, respectively. The DMRG extrapolation errors defined as above are 0.00017, 0.0003, and 0.0003, respectively.

The “exact error”, which we for the sake of the illustration here (where we know the exact energies, which is of course not the case for the cylindrical lattices used in our primary studies of the SS model) define as the difference between extrapolated value based on three data points and the exact energy, are 0.00022, 0.0008, 0.0007, respectively. If the fitting function is switched to a second order polynomial (including the linear term), the extrapolated results using all four  $m$  points go slightly below the exact energies for all three states. Overall, we again found that the higher-order polynomials without the linear terms describe the data better.

The above example shows that the estimated extrapolation errors are of the same magnitude as the “exact errors”. Here the minimum available discarded weight, corresponding to

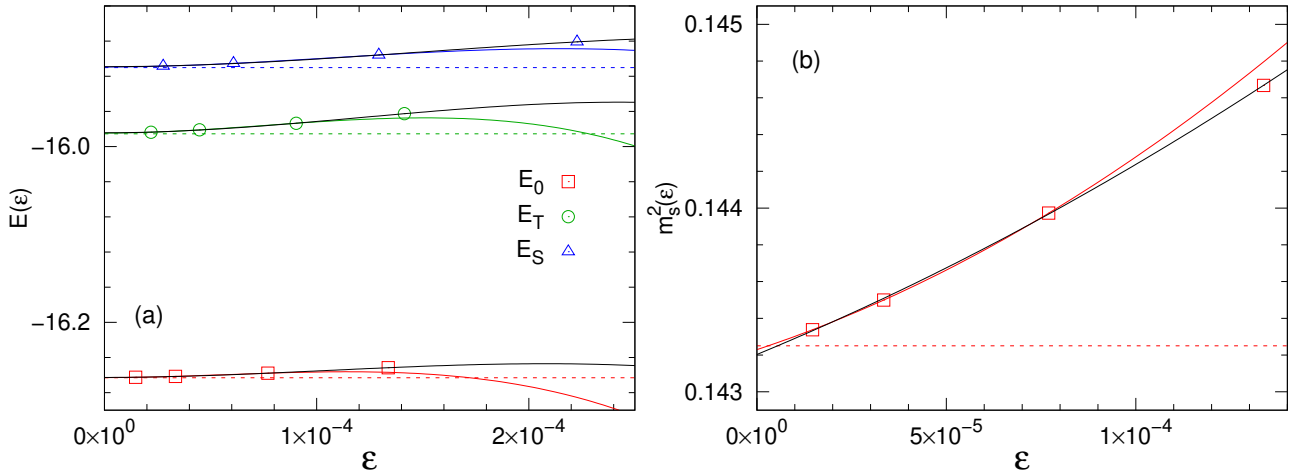


Figure S4. Exact and DMRG results for the  $6 \times 6$  periodic SS lattice at  $g = 0.80$ . (a) DMRG energies of the ground state and first excited state in the singlet and triplet sectors vs the discarded weight  $\epsilon$ , obtained with bond dimension  $m = 800, 1200, 2000$ , and  $3000$ . The colored dashed lines are the corresponding eigenvalues obtained by Lanczos exact diagonalization. The colored solid curves show fits to the form  $E = a + b\epsilon^2 + c\epsilon^3$  using the three points with smallest  $\epsilon$ . The black solid curves show fits to the same functional form using all four points. Their difference in the  $\epsilon \rightarrow 0$  extrapolated values defines the DMRG error of the energy. (b) The staggered magnetization of the ground state. Colored (black) solid curves show fits to the quadratic functions  $m_s^2 = a + b\epsilon + c\epsilon^2$  using three (four) points, and their extrapolation difference defines the DMRG error of the staggered magnetization. The red dashed line shows the exact value.

$m = 3000$  is  $\epsilon \approx 2 \times 10^{-5}$ . This  $\epsilon$  is much larger than the truncation errors reached with larger  $m$  in cylinder systems for  $L \leq 10$  and is comparable with the  $\epsilon$  value reached for  $L \geq 12$ , as seen in Fig. S1. The way the energies flatten out for the cylindrical systems when  $\epsilon$  decreases is very similar to what we observe for the  $6 \times 6$  system, and we see no reason why the results should not have reached  $\epsilon$  small enough to perform the extrapolations as explained.

Figure S4(b) shows extrapolations of the staggered magnetization  $m_s^2(\epsilon)$  in the ground state for which the energies are shown in Fig. S4(a). Here the fitting function is a regular second-order polynomial,  $m_s^2 = a + b\epsilon + c\epsilon^2$ . The error of the order parameter is again defined as the difference between extrapolated values using either the three largest  $m$  points or all four points. The exact value from the Lanczos exact diagonalization is  $m_s^2 = 0.143250$ . The error of the DMRG extrapolation is 0.000026 in this case, and the “exact error” as defined above is 0.000021. We again see that the defined extrapolation error is very reasonable.

All finite-size errors of the results discussed in the main paper were estimated as above, but in most cases the error bars are much smaller than the graph symbols and are not shown explicitly. In the extrapolations to infinite size, the finite-size errors were propagated in the standard way in the function fits, and the resulting error bars are displayed in some of the figures.

## 2. Role of cylinder edges

As shown in Fig. 1 in the main paper, the PS ordering pattern is unique on the cylindrical lattices used here. The cylinder edges act as a  $\mathbb{Z}_2$  symmetry-breaking “pinning field”, allowing us to study the PS order parameter  $m_p$  directly, instead of using the squared order parameter in a system with unbroken symmetry. This approach was discussed in detail in Ref. 38 in the context of a different system, and it was argued that it is the best way to study the order parameters of “singletized” phases with methods that use symmetry-breaking boundary conditions.

Fig. S5 shows examples of the singlet pattern forming on two different lattices, of size  $L = 6$  and  $L = 10$ , both inside the PS phase at  $g = 0.75$  and in the SL phase at  $g = 0.80$ . In the PS phase, we can observe that the alternating pattern of strong and weak empty plaquettes (those without the SS diagonal couplings  $J'$ ) is much stronger in the larger systems. This order enhancement with increasing  $L$  in the PS phase was already seen in the size dependent  $m_p$ , defined as the difference between central adjacent empty plaquettes, in the inset of Fig. 5 in the main paper. The strengthening of the PS order clearly reflects the diminishing quantum fluctuations when long-range order is established with increasing system size in the presence of the symmetry-breaking edge field. Note that the edge order also strengthens with increasing  $L$ .

Turning now to the results in the SL phase, Fig. S5(c) and S5(d), here as well we observe how the edge order is significantly stronger in the larger system. The bulk order parameter, defined in the center of the system, is also stronger in the larger system. However, as seen in the inset of Fig. 5 in the main paper, for the largest system size considered for  $g = 0.80$ ,  $L = 14$ ,  $m_p$  has turned downward [and this is even more clear at  $g = 0.82$  as also illustrated by the results in Fig. S3(c)]. This nonmonotonic behavior outside the PS phase can naturally be explained as a competition between the

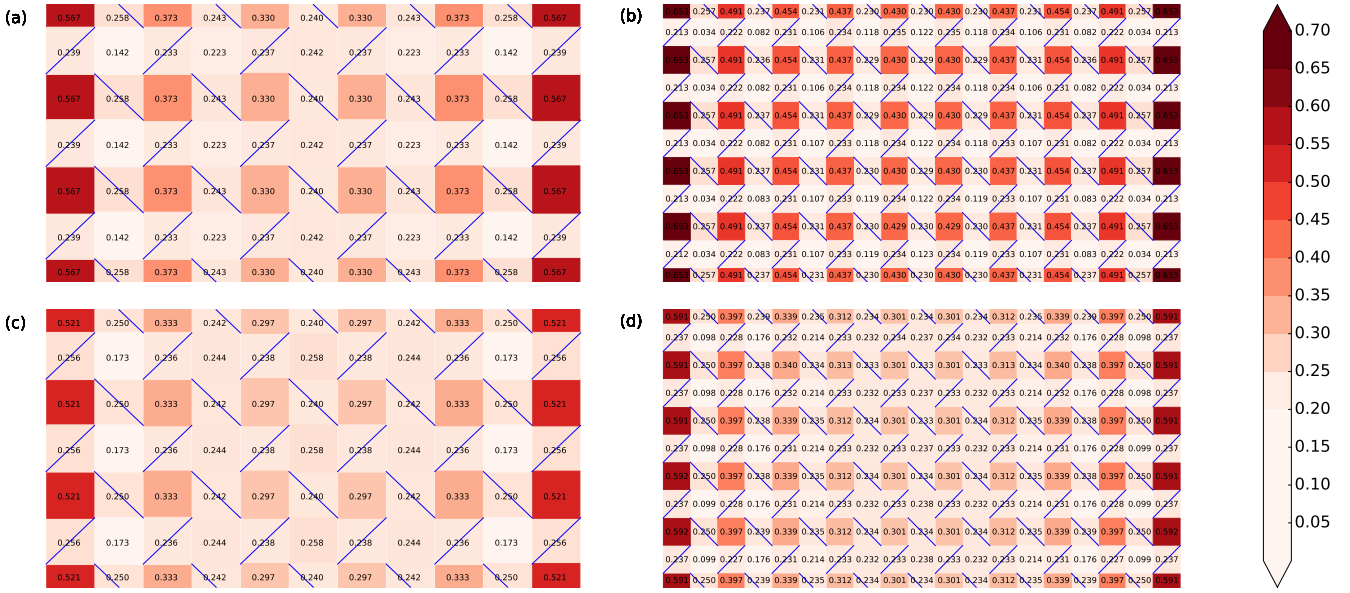


Figure S5. Landscape of plaquette singlet strengths in systems of size  $L = 6$  (left) and  $L = 10$  (right), for  $g = 0.75$  (inside the PS phase) in (a) and (b), and for  $g = 0.80$  (in the SL phase) in (c) and (d). The colored squares correspond to the expectation value  $\langle Q_{\mathbf{R}} \rangle$  of the plaquette operator defined in the main paper for the plaquettes at lattice coordinate  $\mathbf{R}$ . The SS dimer couplings  $J'$  are indicated with the blue lines. In addition to the color coding shown on the vertical bar, the actual numerical values of  $\langle Q_{\mathbf{R}} \rangle$  are also displayed inside each square.

always present (for any  $g$ ) symmetry breaking at the cylinder edge and the decay of this “artificial” induced order in the central part of the system as  $L$  increases. The initial increase with  $L$  for small systems is due to the strengthening of the edge order with  $L$  even when the system is in the SL or AF phase. The eventual down-turn of the order parameter for larger systems is a sign of this edge effect not extending to the bulk, i.e., that the system is not in the PS phase.

It is difficult to imagine any realistic mechanism that would cause  $m_p$  to turn back up as  $L$  increases further after the peak value has been reached and  $m_p$  has begun to decrease with  $L$ . Therefore, we regard the observation of a maximum in  $m_p$  for a given  $L$  as a definite indicator of the system not being in the PS phase. Our results for  $g = 0.80$ -0.84 in Fig. 5 all exemplify this behavior.

### 3. Spin structure factor

In an early field-theoretical study of the SS model within the framework of  $1/S_i$  expansions ( $S_i$  being the spin quantum number of the individual spins) [67], several exotic phases were found in the plane  $(g, 1/S_i)$ , including a gapped SL and a phase with helical magnetic order. The gapped SL is located close to a PS state but not between the PS and AF states as we have found here in the case of the gapless SL. The AF, PS, SL, and helical phases meet at a point, which should be contrasted with our proposed unified phase diagram for DQCPs adjacent to gapless SL phase in Fig. 6, where the PS, AF, and gapless SL phases meet at a DQCP (or possibly a triple point of first-order transitions).

The SL phase of Ref. 67 also hosts short-range helical spin

order. The proposed helical phase and the helical correlations of the gapped SL phase prompts us to investigate the possibility of helical spin correlations in the gapless SL phase identified in the phase diagram of the SS model in the present work. To this end, we have calculated the static spin structure factor  $S(\mathbf{k})$  based on the spin correlation functions  $\langle \mathbf{S}_i \cdot \mathbf{S}_j \rangle$  for all spins  $i, j$  within the central  $L \times L$  square of sites on the cylindrical  $2L \times L$  lattices, defining

$$S(\mathbf{k}) = \frac{1}{L^2} \sum_{i,j} e^{-i\mathbf{k} \cdot (\mathbf{r}_i - \mathbf{r}_j)} \langle \mathbf{S}_i \cdot \mathbf{S}_j \rangle. \quad (S1)$$

In a periodic  $L \times L$  system the wave-vectors should take the form  $k_a = n_a 2\pi/L$ , for  $a \in \{x, y\}$  and  $n_a \in \{0, \dots, L-1\}$ . However, since we do not have periodic boundaries in the  $x$  direction, we can evaluate the Fourier transform for any  $k_x \in [0, 2\pi]$ . To obtain a smooth representation of the structure factor in the 2D  $k$  space, we also use a large number of values for  $k_y$  between the discrete points in principle allowed by the lattice geometry. Because of the periodicity in  $k$ -space we limit the values to  $k_x, k_y \in [0, \pi]$ .

In Fig. S6 we show results for  $L = 10$  systems at three values of the coupling ratio, representing the PS, ( $g = 0.72$ ), SL ( $g = 0.80$ ), and AF ( $g = 0.88$ ) phases. In all cases we observe that the structure factor is peaked at  $\mathbf{k} = (\pi, \pi)$  indicating that the correlations are of the Néel AF type in all phases.

Given the rather small lattice size, we can of course not rigorously rule out order or dominant short-range correlations at  $\mathbf{k} = (\pi, q)$  or  $\mathbf{k} = (q, \pi)$  (where the cylindrical lattices would favor one case) with  $q$  very close to  $\pi$ , but we find such a scenario unlikely.

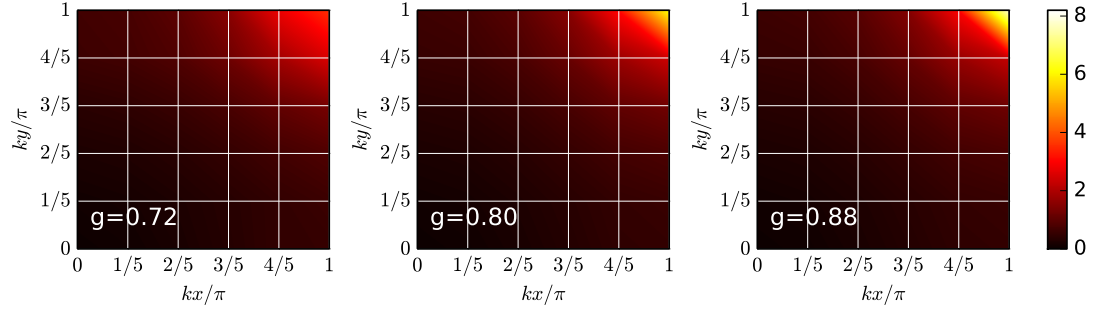


Figure S6. The spin structure defined in Eq. (S1) for  $L = 10$  SS lattices at three different  $g$  values as indicated. The slightly broken  $k_x \leftrightarrow k_y$  reflection symmetry is due to the cylindrical  $N = 2L \times L$  lattice geometry, that is manifested even when the structure is factor defined only on the central  $L \times L$  sites according to Eq. (S1). The symmetry is gradually restored for increasing  $L$ .